Single Ion Implantation and Deterministic Doping

Thomas Schenkel[1],
Ion Beam Technology Group, Accelerator and Fusion Research Division,
Lawrence Berkeley National Laboratory, Berkeley, CA 94720

1. Introduction

The presence of single atoms, e. g. dopant atoms, in sub-100 nm scale electronic devices can affect the device characteristics, such as the threshold voltage of transistors [1, 2], or the sub-threshold currents [3-5]. Fluctuations of the number of dopant atoms thus poses a complication for transistor scaling [1]. In a complementary view, new opportunities emerge when novel functionality can be implemented in devices deterministically doped with single atoms. The grand price of the latter might be a large scale quantum computer, where quantum bits (qubits) are encoded e. g. in the spin states of electrons and nuclei of single dopant atoms in silicon [6], or in color centers in diamond [7, 8]. Both the possible detrimental effects of dopant fluctuations and single atom device ideas motivate the development of reliable single atom doping techniques which are the subject of this chapter.

Single atom doping can be approached with top down and bottom up techniques. Top down refers to the placement of dopant atoms into a more or less structured matrix environment, like a transistor in silicon [9, 10]. Bottom up refers to approaches to introduce single dopant atoms during the growth of the host matrix e. g. by directed self-assembly and scanning probe assisted lithography [11, 12]. Bottom up approaches are discussed in Chapter XYZ.

Since the late 1960'ies, ion implantation has been a widely used technique to introduce dopant atoms into silicon and other materials in order to modify their electronic properties [13]. It works particularly well in silicon since the damage to the crystal lattice that is induced by ion implantation can be repaired by thermal annealing. In addition, the introduced dopant atoms can be incorporated with high efficiency into lattice position in the silicon host crystal which makes them electrically active. This is not the case for e. g. diamond, which makes ion implantation doping to engineer the electrical properties of diamond, especially for n-type doping much harder then for silicon [14, 15].

Ion implantation is usually a highly statistical process, where high fluences of energetic ions, ranging from ~10^9 to >10^{16} cm^{-2} are implanted. For single atom device development, control over the absolute number of ions is needed and ions have to be placed with high spatial resolution. In the following sections we will discuss a series of approaches to single ion implantation with regard to single ion impact sensing and control of single ion positioning.

2. Placement of Single Ions

In an ideal single ion implanter, individual ions of any element are delivered into a controlled area on a wafer at a reasonable rate, each ion impact is registered, and the ion beam is turned off fast enough to prevent impact of the next ion before the sample has been moved to the next implant position. Direct write techniques such as sequential single ion implantation are generally too slow for mass production of e. g. integrated

[1] Email: T_Schenkel@LBL.gov; http://www-ebit.lbl.gov/publications.php

circuit components, but a rate of only a few ions per second suffices for the fabrication of test components in quantum computer development and even for devices scaled to a few thousand qubits.

The effective spatial resolution, x_{eff} , in the formation of electrically active single dopant atom arrays is determined by the beam spot size, x_{beam}, straggling of the implanted ion during slowdown in the target, $x_{straggl}$, and finally by diffusion in consecutive processing steps, such as annealing and gate oxide growth or deposition, x_{diff}. For a donor spin qubit spacing d, with d= 10 to 20 nm in the original Kane proposal for a silicon based quantum computer [6] and d ~100 nm in several variations, the effective resolution in phosphorus atom spacing should be a faction of the qubit spacing. Qubit spacing is one critical metric and another is coherence. Surfaces and interfaces are often a source of noise that can limit qubit coherence [16]. Placement of donor qubits at greater depth thus protects them from this noise source. But there is a trade-off with the achievable placement precision since epitaxial over-growth or implantation at higher energies is needed to achieve greater depth and these can degrade the effective placement precision due to increased diffusion or range straggling, respectively.

We now briefly discuss strategies for control of the these three placement resolution limiting factors. In a well optimized single ion placement experiment, all contributions have to be addressed in parallel and use e. g. of a beam focused to less then 5 nm spot size is ineffective if dopants have a much larger range straggling or diffuse significantly during annealing.

2. 1. Beam Spot Size

Control of the ion position is addressed in the ion optical column of the implanter. There are two approaches to achieving small, i. e. <10 nm, spot sizes. One is to focus ions to a tight spot using a high brightness ion source, the other is to use a broad beam of ions and define the effective beam spot with a nanometer scale stencil mask.

Commercial focused ion beam or FIB systems can deliver pA currents of ions from liquid metal ion guns - mostly Ga^+ - with kinetic energies of ~30 keV into beam spots with diameters of about 5 to 10 nm [17, 25]. Shinada et al have reported focusing of a 60 keV phosphorus ion beam with an aiming accuracy of 60 nm [2]. Here, the phosphorus ions were formed from a liquid metal ion source with a phosphorus containing nickel alloy. Greater variability in the ion species for focused ion beams is highly desired and is being addressed e. g. in the recent development of ion-trap based ion sources [18]. Very low ion temperatures in the laser cooled ion traps and very small virtual source sizes result in ultra-high brightness ion beams that could enable highly precise ion implantation.

Alternatively, beams of low energy dopant ions can be collimated in nano-stencils which can be integrated with a scanning probe as a dynamic shadow masks [19]. Figure 1 shows a schematic of a setup that integrates ion beams with a scanning force microscope. The scanning probe provides imaging and alignment functions, and the nano-stencil limits the effective beam spot size. Nano-stencils with diameters as small as 5 nm have been formed in silicon based cantilevers [19, 32] using a combination of Ga-FIB drilling and local thin film deposition [20].

2. 2. Range Straggling

Range straggling quantifies the lateral and longitudinal spread of the distribution of implanted ions [13]. Range straggling results from statistical energy loss processes during the slowdown of impinging ions. Ion ranges and range straggling can be estimated with the widely used SRIM code [21] and quantified using Secondary Ion Mass Spectrometry. For phosphorus in silicon straggling amounts to ~35 nm for a 60 keV implant with a 70 nm range. For an implantation energy of 10 keV the range is about 15 nm with a longitudinal straggle of 8 nm, and for 1 keV both range and straggling are only a couple of nm. Straggling thus sets a limit to the kinetic energy at which an effective implant resolution can be achieved. A consequence of reducing the impact energy is that single ion registration through detection of secondary electrons becomes impractical in a regime of kinetic electron emission because of the decrease of secondary electron yields [22]. Use of highly charged projectiles avoids this limitation as electron emission following impact of low energy, high charge state ions results from deposition of potential energy, not kinetic energy [23]. For implantation into a given depth, straggling is lower for heavier ions then for lighter ions (see Fig. 2). E. g. for implantation of donors into silicon at a peak depth of about 20 nm, the straggling for 13 keV ^{31}P ions is ~10 nm, while for ^{121}Sb at 25 keV straggling is only about 6 nm.

While useful for quick estimates, SRIM does not include channeling effects, nor effects of accumulated damage on the range of ions.

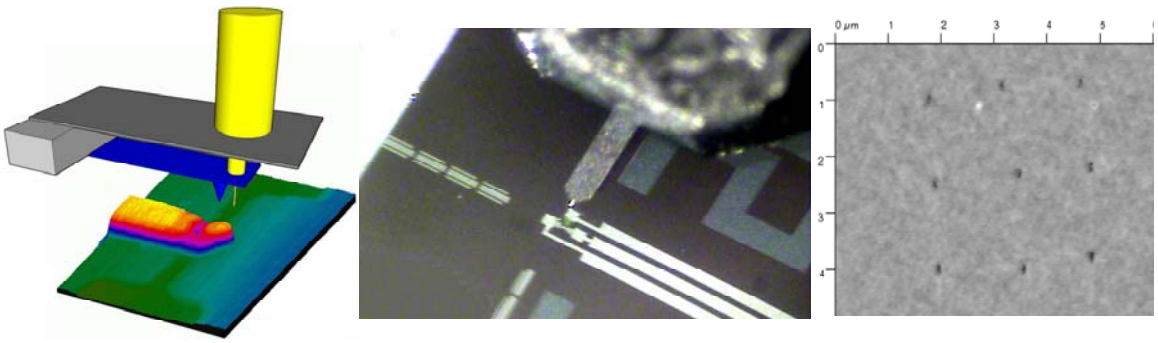

Figure 1: Schematic (left) and photograph (right) of setup for ion implantation with scanning probe alignment and example of pattern formed by ion implantation with scanning probe alignment [24, 25].

2. 3. Diffusion During Annealing

Ion implantation damages the host material because ions transfer momentum to target atoms during the collision cascade as they slow down. In silicon, damage above the amoprphization threshold can be repaired by annealing above 550º C [13, 26]. In diamond, damage above a threshold results in graphitization upon annealing, and there is no epitaxial re-growth as in silicon, making ion implantation doping of diamond much more challenging then for silicon [14]. Besides damage repair, annealing is needed to electrically activate dopants, i. e. to incorporate them into the host lattice. Dopants diffuse through coupling to defects, interstitials and vacancies, which are present as a result of the implant process or which are generated at an equilibrium rate during annealing at a given temperature. Further, defects can also be injected from interfaces or

during annealing in reactive environments [27]. E. g. annealing of silicon under oxidizing conditions results in injection of interstitials. Phosphorus is an interstitial diffuser and oxidation enhanced diffusion can lead to dopant segregation to the SiO_2/Si interface and to dopant loss. Both effects are detrimental to single atom placement, where the position of single dopant atoms should be determined by the spot size of the focused beam or the collimating aperture and where dopant movement has to be minimized while 100% efficient electrical activation is required for efficient single atom device integration. Values for intrinsic and bulk diffusivities, e. g. $D_0=10^{-14}$ cm^2/s for P in Si at 1000 ºC predict a minimal broadening of the implant profile during a few second long annealing step, t, $x_{diff} = 2\sqrt{D_0\ t}$, of only a few nanometers. But dopant movement for shallow implants is often dominated by defect injection form the interface. Antimony is a vacancy diffuser and Sb movement is suppressed during annealing in the presence of an oxide interface in silicon [16]. For dopant atoms in silicon, very high electrical activation efficiencies are routinely achieved [13, 27]. For color center formation in diamond, process development is much less mature and more complicated process sequences are required in order to achieve highly efficient color center formation, e. g. involving cold implantation of nitrogen ions followed by co-implantation of other ions (e. g. carbon or noble gases) at controlled sample temperatures (hot or cold) to increase the vacancy density followed by rapid thermal annealing for NV-center formation [14, 15, 28].

Placement limiting factor	Comment	references
Ion beam spot size	Focused ion beams or dynamic nano-stencil	17, 18, 19
Range straggling	Increases with implant energy, decreases with mass of implanted ion	13, 21
Diffusion during annealing	Dopant specific diffusion mechanisms, surface and interface effects	13, 26, 27

Table 1: Summary of factors limiting placement of single dopant atoms by ion implantation.

2. 4. Examples of characterization of range straggling and diffusion

One atom in a transistor channel volume of 10x10x10 nm^3 is equivalent to a bulk concentration of 10^{18} atoms/cm^3 and many materials analysis techniques that are typically used for analysis of impurities at higher concentrations are also very useful when the goal is to master the placement and integration of single atoms.

Dynamic SIMS (Secondary Ion Mass Spectrometry) is a widely used metrology tool for characterization of depth profiles of implanted ions [29], while Spreading Resistance Analysis (SRA) is widely used for depth profiling of the electrical resistivity of samples, often after ion implantation and annealing [30]. SIMS is sensitive to trace concentrations of elements down to the ppb level (parts per billion, where 1 ppb = $5x10^{13}$ atoms/cm^3 in Silicon). SRA provides no elemental sensitivity, only the sign of the carrier

concentration, and is sensitive to carrier concentrations as low as a ~10^{11} cm^{-3}. Both SIMS and SRA can provide depth profiles with a few nm depth resolution, with SIMS providing higher depth resolution then SRA for high enough concentrations of impurities. Often here are tradeoffs between achievable depth resolution and sensitivity. Figure 2 (top) shows SIMS depth profiles of P atoms in silicon before and after annealing. The SIMS spectra are relatively noisy, even though the P atom peak concentration is above 10^{16} atoms/cm^3. This is due to possible mass interferences, which necessitates running of the SIMS analysis at very high mass resolution, which reduces signal levels at a given depth resolution [31]. The profile taken after rapid thermal annealing in a nitrogen ambient and in the presence of an oxide shown an effect of segregation of ^{31}P atoms to the SiO_2-Si interface. Figure 2 b) (center) shows SIMS depth profiles for similar implant and annealing conditions but for ^{121}Sb ions. The higher ion mass leads to a shallower implant range and lower range straggling, and no dopant segregation is observed. Figure 2 c) further illustrates the effect of higher ion mass in reducing straggling for a given implant energy with a 60 keV Bismuth implant (^{209}Bi) before and after annealing. The SIMS profile also indicates that a small degree of redistribution of bismuth atoms during annealing (1000º C, 10 s). This is unexpected on the basis of low Bi diffusivity values and might be a result of the intense lattice damage induced by the heavy bismuth ions.

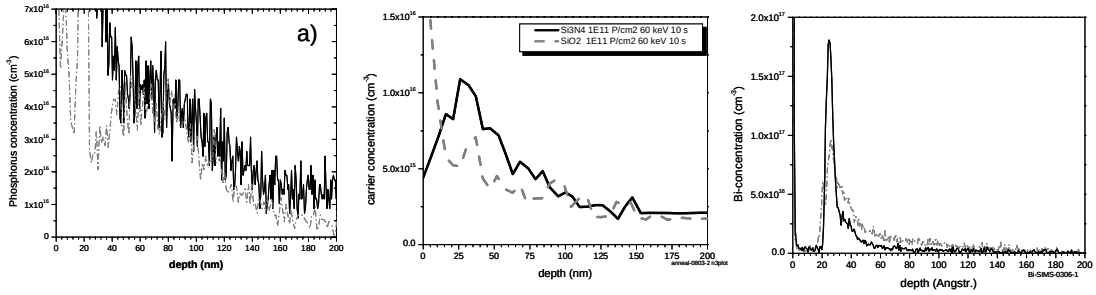

Figure 2: SIMS depth profiles of as-implanted and annealed silicon samples top: ^{31}P (annealed for 10 s at 950 C) [31, 39], middle: ^{121}Sb, annealed for 10 s at 850 C. The vertical line at 10 nm indicates the interface between the top SiO_2 layer and silicon. Bottom: ^{209}Bi, implant before and after annealing (1000 C, 10 s) [31]. The implant energy was 60 keV and the implantation fluence was 2×10^{11} cm^{-2} for all three ion species.

3. Detection of single ions

The ease or difficulty of single ion detection depend on the ions kinetic energy and charge state. For precise single ion placement, kinetic energies have to be low, so that the positioning uncertainty from range straggling remains smaller then a characteristic device scale, such as the nearest neighbor qubit coupling distance. When ions impinge on solids, secondary electrons are emitted, electron-hole pairs are generated inside the solid when the ion transfers its kinetic energy in elastic and inelastic collisions, target material is sputtered off the surface into vacuum and the surface topography can be modified. In some materials, light is emitted in radiative relaxation processes following electronic excitation of target atoms and molecules. Also, X-rays can be emitted following inner-shell ionization of target atoms. For some materials (e. g. graphite, mica and diamond), the problem of single ion detection has been addressed by imaging of

topological modifications, i. e. extended defects, generated on surfaces by single ion impacts.

Method for single ion impact detection	Comment	References
Secondary electrons	Secondary electron yields increase with increasing ion kinetic energy and charge state, and with decreasing surface work functions	2, 10, 32
Electron-hole pairs	Requires integration with diode structures, signal increases with kinetic energy of ions	9
Current changes in transport channels	Requires integration with transport channels (resistors or transistors)	33, 34
Topology modification	Requires high resolution in situ imaging and flat sample surfaces	35, 40

Table 2: Summary of methods for single ion impact detection

Figure 3 shows an example of single ion impact detection through measurements of current changes in transistor channels [24]. Transistors were processed with tungsten metallization for post implant annealing and holes in the transistor channels were opened using a combination of focused ion drilling and reactive gas etching in a dual beam FIB [33]. Scanning the dynamic shadow mask over the transistor results in a response map, similar to ion beam induced charge mapping (which is usually done with MeV ion beams [36] with micron scale imaging resolution limits). An example of an ion impact response map is shown in Figure 4. This method can be applied for studies of the response of scaled device components to ionizing radiation at a spatial resolution limited by the opening diameter of the nano-stencil (80 nm in the example of Figure 4). Transistors like these have been used for electrical detection of spin resonance [37]. Thus the same device structure is used for single ion impact detection and, after annealing, for electrical detection of spin resonance. Scaling to single spin state readout is subject of ongoing research [38].

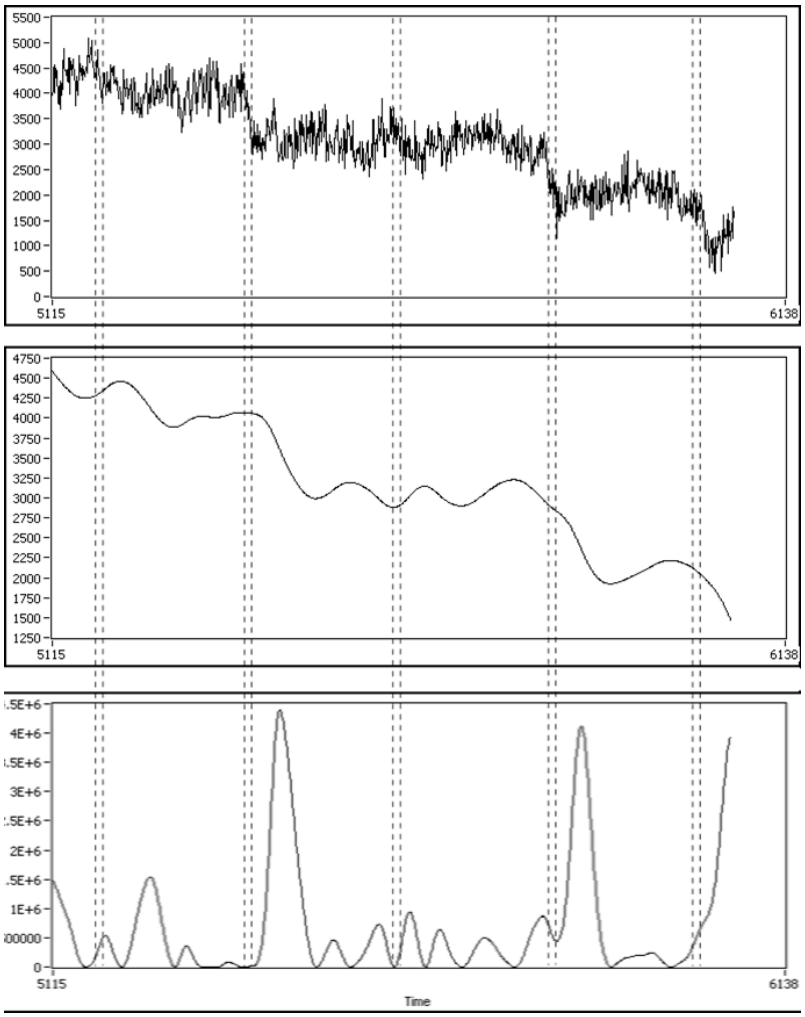

FIG. 3: Source-drain current as a function of time during pulsed exposure of a transistor to Xe^{6+} ions, E_{kin}=48 keV, a) raw data, b) smoothed data, and c) derivative of b), with current steps induced by single ion impacts at room temperature [28].

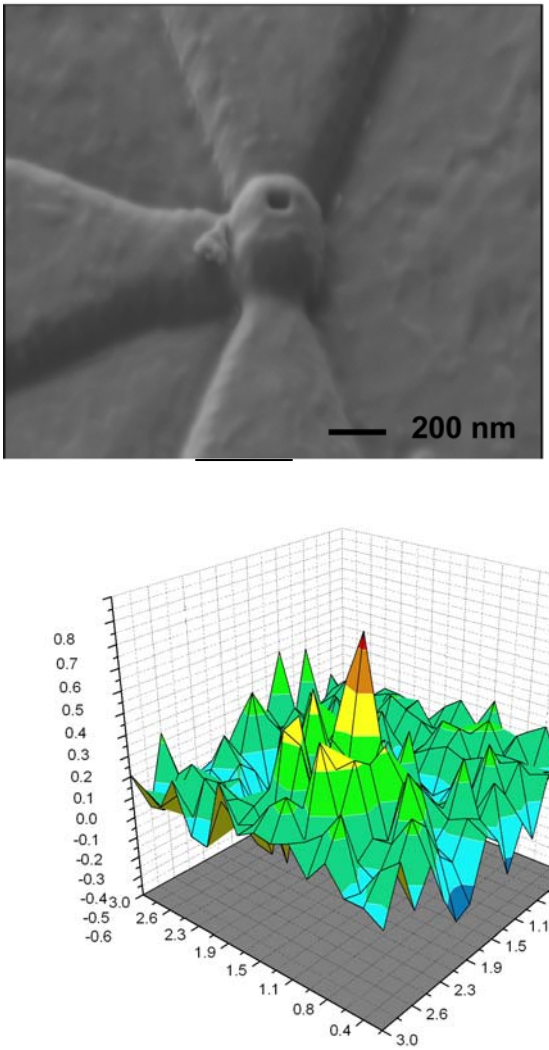

Figure 4: Scanning electron micrograph (top) and ion impact response map (bottom) from a FinFet with 100 nm hole in the top gate [24, 31].

4. Outlook

As lithographic access to sub-25 nm scale features becomes more an more routine in many laboratories, effects of single atoms on process variability and function in device structures will become more and more common. This poses challenges and opportunities. Techniques for deterministic doping of nanoscale structures with single dopant atoms enable paths for understanding of single atom effects both where they are undesired (e. g. random dopant fluctuations in scaled transistors) and where they offer tantalizing new opportunities (e. g. in single atom based quantum bits and quantum computer development).

References

[1] R. W. Keyes, Rep. Prog. Phys. **68**, 2701 (2005)
[2] T. Shinada, S. Okamoto, T. Kobayashi, and I. Ohdomari, Nature 437, 1128 (2005)
[3] H. Sellier, G. P. Lansbergen, J. Caro, S. Rogge, N. Collaert, I. Ferain, M. Jurczak, and

S. Biesemans, Phys. Rev. Lett. **97**, 206805 (2006)
[4] Y. Ono, K. Nishiguchi, A. Fujiwara, H. Yamaguchi, H. Inokawa, and Y. Takahashi, Appl. Phys. Lett. **90**, 102106 (2007)
[5] L. E. Calvet, R. G. Wheeler, and M. A. Reed, Phys. Rev. Lett. **98**, 096805 [2007]
[6] B. E. Kane, Nature 393, 133-137 (1998)
[7] F. Jelezko, T. Gaebel, I. Popa, M. Domhan, A. Gruber, and J. Wrachtrup, Phys. Rev. Lett. 93, 130501 (2004);
[8] G. D. Fuchs, V. V. Dobrovitski, R. Hanson, A. Batra, C. D. Weis, T. Schenkel, and D. D. Awschalom, Phys. Rev. Lett. 101, 117601 (2008)
[9] D. N. Jamieson, et al., Appl. Phys. Lett. 86, 202101-202103 (2005)
[10] T. Schenkel, et al., J. Appl. Phys. 94, 7017-7024 (2003)
[11] T. C. Shen, J. S. Kline, T. Schenkel, S. J. Robinson, J. Y. Ji, C. Yang, R. R. Du, and J. R. Tucker, J. Vac. Sci. Tech. B 22, 3182 (2004)
[12] R. J. Ruess, B. Weber, K. E. J. Goh, O. Klochan, A. R. Hamilton, M. Y. Simmons, Phys. Rev. B 76, 085403 (2007)
[13] M. Nastasi and J. W. Mayer, "Ion Implantation and Synthesis of Materials", (Springer, New York, 2006)
[14] J. F. Prins, Semic. Sc. Tech. 18, S27 (2003)
[15] R. Kalish, Semiconductors and Semimetals 76, 145 (2003)
[16] T. Schenkel, A. M. Tyryshkin, R. deSousa, K. B. Whaley, J. Bokor, J. A. Liddle, A. Persaud, J. Shangkuan, I. Chakarov, and S. A. Lyon, Appl. Phys. Lett. 88, 112101 (2006)
[17] J. Orloff, M. Utlaut, and L. Swanson, "High Resolution Focused Ion Beams", (Kluwer, New York, 2003)
[18] W. Schnitzler, N. M. Linke, R. Fickler, J. Meijer, F. Schmidt-Kaler, K. Singer, Phys. Rev. Lett. 102, 070501 (2009)
[19] A. Persaud, S. J. Park, J. A. Liddle, J. Bokor, I. W. Rangelow, and T. Schenkel, NanoLetters 6, 1087-1091 (2005)
[20] T. Schenkel, V. Radmilovic, E.A. Stach, S.-J. Park and A. Persaud, J. Vac. Sci. Technol. B 21, 2720 (2003)
[21] J. F. Ziegler, Nucl. Instr. Meth. B 219, 1027 (2004); www.srim.org
[22] R. A. Baragiola, Nucl. Instr. Meth. B 78, 223 (1993)
[23] A. Arnau et al., Surf. Sci. Reports 27, 117 (1997)
[24] C. D. Weis, A. Schuh, A. Batra, A. Persaud, I. W. Rangelow, J. Bokor, C. C. Lo, S. Cabrini, D. Olynick, S. Duhey, and T. Schenkel, Nucl. Instr. Meth. B 267, 1222 (2009)
[25] W. J. Moberly Chan, et al., MRS BULLETIN 32, 424 (2007)
[26] V. E. Borisenko and P. J. Hesketh, "Rapid Thermal Processing of Semiconductors", (Plenum, New York, 1997)
[27] A. Ural, P. B. Griffin, J. D. Plummer, J. Appl. Phys. 85, 6440 (1999)
[28] C. D. Weis, A. Schuh, A. Batra, A. Persaud, I. W. Rangelow, J. Bokor, C. C. Lo, S. Cabrini, E. Sideras-Haddad, G. D. Fuchs, R. Hanson, D. D. Awschalom, and T. Schenkel, J. Vac. Sci. Techn. B 26, 2596 (2009)
[29] C. R. Brundle, C. A. Evans, and S. Wilson, "Encyclopedia of materials characterization", (Butterworth-Heinemann, Boston, 1992)
[30] D. H. Dickey, J. Vac. Sci. Technol. B 20, 467 (2002); www.solecon.com

[31] T. Schenkel, C. C. Lo, C. D. Weis, A. Schuh, A. Persaud, and J. Bokor, Nucl. Instr. Meth. B 267, 2563 (2009)
[32] A. Persaud, J. A. Liddle, J. Bokor, T. Ivanov, I. Rangelow, and T. Schenkel, J. Vac. Sci. Technol. B, 23, 2798 (2005)
[33] A. Batra, C. D. Weis, J. Reijonen, A. Persaud, S. Cabrini, C. C. Lo, J. Bokor and T. Schenkel, Appl. Phys. Lett. 91, 193502 (2007)
[34] T. Shinada, T. Kurosawa, H. Nakayama, Y. Zhu, M. Hori, I. Ohdomari, Nanotechnology 19, 34502 (2008)
[35] E. Sideras-Haddad, T. Schenkel, D.B. Rebuli, A. Persaud, S. Shrivastava, D.H. Schneider, B. Mwakikunga, Nucl. Instr. Meth. B 256, 464 (2007); E. Sideras-Haddad, et al., Nucl. Instr. Meth. B 267, 2774 (2009)
[36] M. B. H. Breese, V. E. Vittone, G. Vizkelethy, P. J. Sellin, Nucl. Instr. Meth. B 264, 345 (2007)
[37] C. C. Lo, J. Bokor, T. Schenkel, J. He, A. M. Tyryshkin, and S.A. Lyon, Appl. Phys. Lett. 91, 242106 (2007)
[38] M. Sarovar, K. C. Young, T. Schenkel, K. B. Whaley, Phys. Rev. B 78, 245302 (2008)
[39] S.-J. Park, A. Persaud, J. A. Liddle, J. Nilsson, J. Bokor, D. H. Schneider, I. Rangelow and T. Schenkel, Microelectronic Engineering 73-74, 695 (2004)
[40] D. Schneider, M.A. Briere, M.W. Clark, J. McDonald, J. Biersack and W. Siekhaus, Surface Science 294, 403 (1993)

A**cknowledgments**

This work was supported by NSA under contract number MOD 713106A, and by the Director, Office of Science, of the Department of Energy under Contract No. DE-AC02-05CH11231.